

Effective index approximations of photonic crystal slabs: a 2-to-1-D assessment

Manfred Hammer · Olena V. Ivanova

Received: 16 July 2009 / Accepted: 4 November 2009 / Published online: 8 December 2009
© The Author(s) 2009. This article is published with open access at Springerlink.com

Abstract The optical properties of slab-like photonic crystals are often discussed on the basis of effective index (EI) approximations, where a 2-D effective refractive index profile replaces the actual 3-D structure. Our aim is to assess this approximation by analogous steps that reduce finite 2-D waveguide Bragg-gratings (to be seen as sections through 3-D PC slabs and membranes) to 1-D problems, which are tractable by common transfer matrix methods. Application of the EI method is disputable in particular in cases where locally no guided modes are supported, as in the holes of a PC membrane. A variational procedure permits to derive suitable effective permittivities even in these cases. Depending on the structural properties, these values can well turn out to be lower than one, or even be negative. Both the “standard” and the variational procedures are compared with reference data, generated by a rigorous 2-D Helmholtz solver, for a series of example structures.

Keywords Integrated optics · Numerical modeling · Photonic crystal slabs · Effective index approximation

M. Hammer · O. V. Ivanova
MESA⁺ Institute for Nanotechnology, University of Twente, Enschede, The Netherlands

M. Hammer (✉)
Department of Applied Mathematics, University of Twente, P.O. Box 217, 7500 AE, Enschede,
The Netherlands
e-mail: m.hammer@math.utwente.nl
URL: <http://www.math.utwente.nl>

O. V. Ivanova
URL: <http://www.math.utwente.nl>
URL: <http://www.utwente.nl/en>
URL: <http://www.mesaplus.utwente.nl>

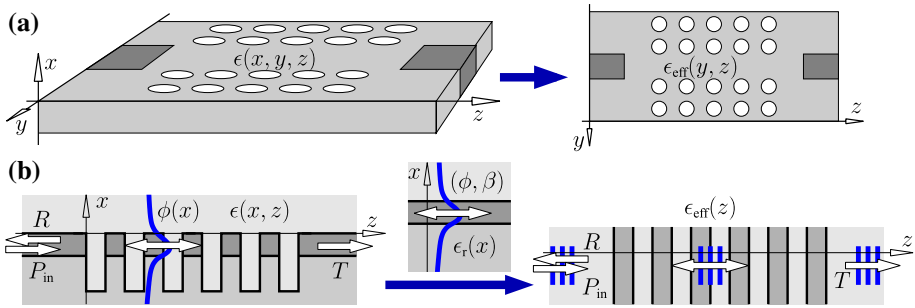


Fig. 1 Effective index reduction of integrated optical scattering problems, schematically. **a** Replacement of a 3-D photonic crystal slab with real permittivity $\epsilon(x, y, z)$ by a 2-D effective permittivity profile $\epsilon_{\text{eff}}(y, z)$. **b** The model problem considered in this paper: the scattering by a 2-D planar waveguide-Bragg grating, given by the dielectric permittivity $\epsilon(x, z)$, is approximated by 1-D plane wave transmission through a multilayer stack with effective permittivity profile $\epsilon_{\text{eff}}(z)$

1 Introduction

The propagation of light through slab-like photonic crystals (PCs) (Prather et al. 2006) is frequently described in terms of effective indices (EIs). One replaces the actual 3-D structure by an effective 2-D refractive index profile, given by the propagation constants of the slab modes of the local vertical refractive index profiles. Though the popular approach is usually introduced for the approximate calculation of waveguide modes (Chiang 1986; van de Velde et al. 1988; Vassallo 1991; Benson et al. 1992; März 1994; Chiang 1996; Okamoto 2000), it is just as well applicable to certain classes of propagation or scattering problems. This concerns not only purposes of qualitative reasoning (Čtyroký 2001; Qiu et al. 2001; Witzens et al. 2002; Shi et al. 2005) but also the actual design of structures (Bienstman et al. 2003; Qiu et al. 2003; Kok et al. 2007), and comparison with / fitting to experimental data (Krauss et al. 1996; Benisty et al. 1999; Qiu et al. 2002). Figure 1a shows the 3-to-2-D reduction schematically.

A study that provides some assessment on the accuracy of the approximations (Qiu et al. 2002) is restricted to band structure calculations, i.e., computations on a single unit cell for in-plane fully periodic structures, due to the computational effort required for the finite-difference time-domain (FDTD) calculations (Taflove and Hagness 2000) that serve to generate the numerical reference data. Yang et al. (2005), Gao and Zhou (2007), Dems and Nakwaski (2006), Zhou et al. (2007), Liu and Panepucci (2008) focus on the EI approach itself, and on possible improvements, in the explicit context of PC slabs. Also here the emphasis is on band structure features (Gao and Zhou 2007; Dems and Nakwaski 2006). Yang et al. (2005), Zhou et al. (2007), Liu and Panepucci (2008) regard the effective index of the non-etched slab regions as a fit parameter to match certain properties of the 2-D band structure to numerical reference calculations. The fitted effective values are then used for further 2-D calculations on non-periodical configurations like waveguide channels or localized cavities (Zhou et al. 2007; Liu and Panepucci 2008), and for the estimation of out-of-plane losses (Liu and Panepucci 2008). It should be mentioned that, as an alternative to the scheme of Fig. 1a, a “side view” variant of a 3-to-2-D dimensionality reduction is possible, which replaces the PC-slab by a 2-D structure similar to the left part of Fig. 1b. A corresponding comparison for the case of Bragg gratings in photonic wires has been carried out in Gnan et al. (2006).

Still, beyond the aforementioned paper, we are so far not aware of any assessment, where the approximation is checked for full devices, including the input and exit transitions to conventional waveguides, and for a certain variety of structures. This is what we would like to provide with the present paper. The computational complexity, however, of rigorous numerical simulations, sufficiently converged for benchmark purposes, on realistic 3-D PC slab devices, even if only moderately sized, renders these computations highly inconvenient at best, if not impractical at all. As illustrated in Fig. 1, we therefore retreat to a lower dimensionality: In place of the 3-D to 2-D EI reduction (a), in line with Čtyroký (2001), Blair and Goeckeritz (2007) we will check the approximation by analogous steps (b) that reduce finite 2-D waveguide Bragg-gratings to 1-D problems. Being equivalent to the plane wave transmission through dielectric multilayer stacks, the latter 1-D problems are conveniently solvable by standard transfer matrix methods. A 2-D Helmholtz solver (Hammer 2007, 2009) allows to solve the original 2-D problems rigorously, i.e., to generate reliable benchmark solutions for the assessment of the quality of the EIM approximation.

What concerns the—not obvious—transfer of the findings to 3-D, one should be aware that the 2-D results, given as functions of coordinates x and z , are exact solutions for 3-D problems, where both the structure, i.e., the permittivity ϵ , and all optical fields are constant along the y axis.¹ We thus simulate what happens if an initially vertically (x) confined, but laterally (y) wide, non-confined beam traverses a series of trenches perpendicular to its direction of propagation z . The field plots shown in this paper, then correspond to vertical cross sections of the real 3-D field along the propagation axis. A structure as in Fig. 1a certainly does not belong to this class. Our model problems consider only vertical features of permittivity and field (including losses due to out of plane radiation (Hadley 2002; Benisty et al. 2000), reference calculations), while lateral variations, i.e., the lateral confinement in the PC channel in Fig. 1a, are disregarded. Nevertheless, x - z cross sections through the PC membrane at positions y , that include the center of a row of holes, resemble closely the 2-D profile considered in Sect. 3.2. One might thus view the 2-to-1-D examples in this paper as a kind of worst case scenario for the accuracy that can be expected from an EI approximation of a real PC slab configuration.

The EI-viewpoint becomes particularly questionable, if locally the vertical refractive index profile cannot accommodate any guided mode, as e.g., in the holes of a PC membrane. It appears to be generally believed that then the background refractive of the respective region (i.e., 1.0 for air holes) is to be used as effective refractive index. For configurations with not too deep holes, where the guiding film is supported by a substrate (or buffer layer of sufficient thickness), the refractive index of that substrate serves as another candidate for the effective index of the hole regions. Frequently this heuristic choice is not even mentioned. A way out can be found by means of a variational view on the EI method (EIM). We will check numerically a recipe (Vassallo 1991; van Groesen and Molenaar 2007) to uniquely define an effective permittivity even for these cases. The procedure increases the computational effort only marginally, when compared to a “standard” EI approach. Based on clear physical assumptions, it also allows to assemble an approximation to the full optical field.

Section 2 provides the theoretical background for this variational effective index method (vEIM). The following Sects. 3.1–3.4, then cover a series of examples, where the quality of the vEIM approximation is discussed along with results of a standard EI treatment. A preliminary account of the present study has been given in Hammer and Ivanova (2008). See Ivanova et al. (2008a), Ivanova et al. (2009b) for outlines of extensions towards rigorous expansions

¹ Quasi 2-D configurations with no or only very weak lateral confinement could be realized by the corrugation of wide rib waveguides with only shallow etching, i.e., by weak lateral refractive index contrast. Applications of such structures are discussed e.g., in Lohmeyer et al. (2001), Lohmeyer and Stoffer (2001).

with multiple vertical basis fields, then with a substantially larger range of applicability, and towards the 3-to-2-D dimensionality reduction of real 3-D PC structures.

2 Variational effective index approximation

Variational techniques have some tradition (Chiang 1986; Benson et al. 1992) in the derivation of EIM-variants (for scalar mode analysis). For consistency reasons, we start with a functional form (Vassallo 1991; Hammer 2007) of the full 3-D Maxwell equations in the frequency domain:

$$\mathcal{F}(\mathbf{E}, \mathbf{H}) = \int \int \int_{\Omega} \{ \mathbf{E} \cdot (\nabla \times \mathbf{H}) + \mathbf{H} \cdot (\nabla \times \mathbf{E}) - i\omega\epsilon_0\epsilon \mathbf{E}^2 + i\omega\mu_0 \mathbf{H}^2 \} dx dy dz. \tag{1}$$

Here ϵ_0 and μ_0 are the vacuum permittivity and permeability. All fields oscillate harmonically $\sim \exp(i\omega t)$ in time with angular frequency $\omega = kc = 2\pi c/\lambda$, usually given in terms of the vacuum wavenumber k and wavelength λ , for vacuum speed of light c . The relative dielectric permittivity $\epsilon(x, y, z)$ encodes the structural information; one assumes a unit relative permeability at the relevant optical frequencies. Stationarity of \mathcal{F} implies that the optical electric field \mathbf{E} and magnetic field \mathbf{H} satisfy the curl equations

$$\nabla \times \mathbf{E} = -i\omega\mu_0\mathbf{H}, \quad \nabla \times \mathbf{H} = i\omega\epsilon_0\epsilon\mathbf{E} \tag{2}$$

within the domain Ω . 2-D configurations as in Fig. 1b with a structure and fields that are constant along y , are covered after omitting the y -integration in the functional (1).

Below we will first restrict the problem and accordingly the functional to polarized planar solutions. Assuming a separable form of the respective principal field component, one arrives at an EIM-like procedure through a second restriction step. The formalism is similar to what has been applied in the context of scalar and vectorial mode solvers in Ivanova et al. (2007, 2008, 2009).

2.1 TE polarization

Transverse electric (TE) polarized solutions \mathbf{E}, \mathbf{H} of Eq. 2 for y -independent permittivity $\epsilon(x, z)$ are usually given in terms of the principal electric field component $E_y(x, z)$:

$$\mathbf{E}(x, z) = \begin{pmatrix} 0 \\ E_y \\ 0 \end{pmatrix}(x, z), \quad \mathbf{H}(x, z) = \frac{i}{\omega\mu_0} \begin{pmatrix} -\partial_z E_y \\ 0 \\ \partial_x E_y \end{pmatrix}(x, z). \tag{3}$$

After insertion of Eq. 3 and without the y -integration, \mathcal{F} becomes a functional (Vassallo 1991; van Groesen 2003; Sopaheluwakan 2006; van Groesen and Molenaar 2007) of the scalar field E_y only:

$$\mathcal{F}(E_y) = \int \int_{\Omega_2} \left\{ (\partial_x E_y)^2 + (\partial_z E_y)^2 - k^2 \epsilon E_y^2 \right\} dx dz. \tag{4}$$

Here continuity of E_y is required, and a constant factor has been omitted. If this restricted functional becomes stationary for E_y , then that field satisfies the standard 2-D Helmholtz equation

$$\partial_x^2 E_y + \partial_z^2 E_y + k^2 \epsilon E_y = 0, \tag{5}$$

everywhere in the 2-D domain Ω_2 . E_y and its partial derivatives are continuous across any discontinuities in ϵ .

As a step towards an EIM-like approximation of Eq. 5 one chooses a 1-D reference permittivity profile $\epsilon_r(x)$ and an associated guided slab mode χ_r and propagation constant β_r , that satisfy the TE slab mode equation

$$\partial_x^2 \chi_r + (k^2 \epsilon_r - \beta_r^2) \chi_r = 0. \tag{6}$$

Central assumption for what follows is that χ_r represents an acceptable approximation for the vertical shape of E_y along the entire z -axis. The principal field can then be given the separable form

$$E_y(x, z) = \chi_r(x) \psi(z), \tag{7}$$

with a yet to be determined function ψ . The physical assumption behind Eq. 7 can be more or less well realized, depending on all properties of the configuration in question. In general, it is not possible to check the validity in another way than by reference calculation, as in this paper.

While the choice of the reference profile and mode is in principle arbitrary, one should be aware that the desired 1-D problem is meant as an approximation of the *open* 2-D problem, where Ω_2 spans the entire x - z -plane. This setting makes physical sense only if the structure in question is a bounded corrugation of an otherwise homogeneous background, possibly with some well defined, outwards homogeneous access channels. In the examples of Sect. 3, these are half-infinite dielectric slab waveguides, and Eq. 7 should be a good approximation of the real field in those input- and output channels in the first place. Consequently that waveguide profile and its fundamental mode are natural candidates for ϵ_r , χ_r , and β_r .

Given those quantities, after insertion of the ansatz Eq. 7, \mathcal{F} becomes a functional of the remaining unknown ψ :

$$\mathcal{F}(\psi) = \int \{(\partial_z \psi)^2 - k^2 \epsilon_{\text{eff}} \psi^2\} dz. \tag{8}$$

Constant factors have been omitted again. The effective permittivity (Vassallo 1991; van Groesen and Molenaar 2007)

$$\epsilon_{\text{eff}} = \frac{\beta_r^2}{k^2} + \frac{\int (\epsilon - \epsilon_r) \chi_r^2 dx}{\int \chi_r^2 dx}, \tag{9}$$

z -dependent through ϵ , now contains the vertically averaged structural information. By looking for conditions for variational stationarity with respect to ψ , one extracts the 1-D equation

$$\partial_z^2 \psi + k^2 \epsilon_{\text{eff}} \psi = 0 \tag{10}$$

for the field dependence on the horizontal coordinate. Continuity of ψ and $\partial_z \psi$ across possible discontinuities in ϵ_{eff} is required.

Equation 9 resembles the familiar expression for the first order propagation constant shift of guided modes according to small uniform bulk perturbations (Vassallo 1991; Lohmeyer 1999). Indeed, the latter expression can be recovered if one considers the wave number $k \sqrt{\epsilon_{\text{eff}}}$ associated with local solutions $\sim \exp(\pm i k \sqrt{\epsilon_{\text{eff}}} z)$ of Eq. 10 for constant ϵ_{eff} , and expands the square root, assuming a small difference $\epsilon - \epsilon_r$. Note that for positions z , where the difference vanishes, ϵ_{eff} equals the square of the effective mode index β_r/k associated with the reference mode. Functions that satisfy Eq. 10, expanded by Eqs. 3, 7 for the full problem,

are thus exact solutions of Eqs. 2 or 5 in those regions. In the examples of Sect. 3 this concerns regions of the non-etched slab. Elsewhere, i.e., in the z -positions of the holes, the formalism predicts a propagation with a wave number that is modified according to the local permittivity perturbation. Clearly, perturbation theory is used at its limits, or even beyond its limits, in the examples of Sect. 3 with strong refractive index contrast.

Obviously, Eqs. 9 and 10 could have been derived alternatively by using the combined ansatz

$$\mathbf{E}(x, z) = \begin{pmatrix} 0 \\ \chi_r(x)\psi(z) \\ 0 \end{pmatrix}, \quad \mathbf{H}(x, z) = \frac{i}{\omega\mu_0} \begin{pmatrix} -\chi_r(x) \partial_z \psi(z) \\ 0 \\ \partial_x \chi_r(x) \psi(z) \end{pmatrix} \tag{11}$$

directly with the 2-D restriction of the vectorial functional 1. Equations 11 thus give a clear recipe on how to extend the primary scalar solution ψ of Eq.10 towards an approximation to the full optical field in the 2-D configuration.

2.2 TM polarization

Analogous expressions can be derived for transverse magnetic (TM) fields. To minimize the notational overhead, we will use the same symbols as before, although their content differs for TM polarization. The principal magnetic field component $H_y(x, z)$ allows to state polarized solutions of Eq. (2) for a 2-D permittivity $\epsilon(x, z)$ in the form

$$\mathbf{E}(x, z) = \frac{i}{\omega\epsilon_0\epsilon} \begin{pmatrix} \partial_z H_y \\ 0 \\ -\partial_x H_y \end{pmatrix} (x, z), \quad \mathbf{H}(x, z) = \begin{pmatrix} 0 \\ H_y \\ 0 \end{pmatrix} (x, z). \tag{12}$$

Restriction of \mathcal{F} , stripped of the y -integral, to the field (12) leads, up to constant factors, to a functional of H_y only:

$$\mathcal{F}(H_y) = \int \int_{\Omega_2} \left\{ \frac{1}{\epsilon} ((\partial_x H_y)^2 + (\partial_z H_y)^2) - k^2 H_y^2 \right\} dx dz. \tag{13}$$

Continuity of H_y is required. If the functional (13) becomes stationary for H_y , then that field satisfies the modified 2-D Helmholtz equation

$$\partial_x \frac{1}{\epsilon} \partial_x H_y + \partial_z \frac{1}{\epsilon} \partial_z H_y + k^2 H_y = 0, \tag{14}$$

everywhere in the 2-D domain Ω_2 . The quantities H_y and $\epsilon^{-1}(\mathbf{n} \cdot \nabla)H_y$ are continuous across any discontinuities in ϵ with normal \mathbf{n} .

The EIM-like approximation of Eq. 14 is initiated by the choice of a 1-D reference permittivity profile $\epsilon_r(x)$ and an associated guided slab mode χ_r and propagation constant β_r , that satisfy the TM slab mode equation

$$\epsilon_r \partial_x \frac{1}{\epsilon_r} \partial_x \chi_r + (k^2 \epsilon_r - \beta_r^2) \chi_r = 0. \tag{15}$$

One assumes that χ_r represents an acceptable approximation for the vertical shape of H_y for all positions z , such that the principal field can be written

$$H_y(x, z) = \chi_r(x) \psi(z), \tag{16}$$

where ψ remains to be determined. The ansatz (16) restricts \mathcal{F} to a functional of ψ only. Up to constant factors (the mode normalization $\int \epsilon_r^{-1} \chi_r^2 dx$ has been introduced for proper scaling), this reads

$$\mathcal{F}(\psi) = \int \left\{ \frac{1}{b} (\partial_z \psi)^2 - k^2 a \psi^2 \right\} dz. \tag{17}$$

The effective structural properties are in this case encoded by the two quantities

$$b = \frac{\int \frac{1}{\epsilon_r} \chi_r^2 dx}{\int \frac{1}{\epsilon} \chi_r^2 dx} \quad \text{and} \quad a = \frac{\beta_r^2}{k^2} + \frac{\int \left(\frac{1}{\epsilon_r} - \frac{1}{\epsilon} \right) (\partial_x \chi_r)^2 dx}{k^2 \int \frac{1}{\epsilon_r} \chi_r^2 dx}. \tag{18}$$

Note that here both a and b are z -dependent due to the presence of ϵ . Requiring variational stationarity with respect to ψ leads to the 1-D equation

$$\partial_z \frac{1}{b} \partial_z \psi + k^2 a \psi = 0. \tag{19}$$

Continuity of ψ and $b^{-1} \partial_z \psi$ across possible discontinuities in a and b is required. If ϵ is piecewise constant (as it is the case for all our examples), then also a and b are piecewise constant along z . Equation (19) can then be given the more familiar form

$$\partial_z^2 \psi + k^2 \epsilon_{\text{eff}} \psi = 0, \tag{20}$$

where the product of a and b determines the local effective permittivity

$$\epsilon_{\text{eff}} = \frac{\beta_r^2}{k^2} \frac{\int \frac{1}{\epsilon_r} \chi_r^2 dx}{\int \frac{1}{\epsilon} \chi_r^2 dx} + \frac{\int \left(\frac{1}{\epsilon_r} - \frac{1}{\epsilon} \right) (\partial_x \chi_r)^2 dx}{k^2 \int \frac{1}{\epsilon_r} \chi_r^2 dx}. \tag{21}$$

Note that we have $\epsilon_{\text{eff}} = (\beta_r/k)^2$ and $b = 1$ at positions z where $\epsilon(x, z) = \epsilon_r(x)$. Solutions of Eqs. 12, 16, 19 satisfy Eq. 2 exactly in these “native” regions of the reference mode χ_r . Elsewhere, i.e., in corrugated regions, Eq. 21 predicts a wave number shift for solutions of Eq. 20 due to the permittivity perturbation. These expressions are somewhat more involved than for TE polarization, in line with the perturbational expressions for the first order shift of propagation constants of planar TM modes due to small uniform bulk perturbations (Lohmeyer 1999) (the permittivity acts on the components of the electric field, of which there are two for TM instead of one as for TE).

Also here Eqs. 19 and 18 can be obtained directly by restricting the original functional Eq. 1 to the ansatz

$$\mathbf{E}(x, z) = \frac{\mathbf{i}}{\omega \epsilon_0 \epsilon} \begin{pmatrix} \chi_r(x) \partial_z \psi(z) \\ 0 \\ -\partial_x \chi_r(x) \psi(z) \end{pmatrix}, \quad \mathbf{H}(x, z) = \begin{pmatrix} 0 \\ \chi_r(x) \psi(z) \\ 0 \end{pmatrix}. \tag{22}$$

2.3 Comments

Equations 10 and 20 govern the 1-D propagation of light through a dielectric multilayer stack with permittivity $\epsilon_{\text{eff}}(z)$. One has thus replaced the original 2-D problem by an effective 1-D problem, where the structural information associated with the missing spatial dimension has been transferred into the expression for the effective permittivity. Below we refer to the

computational approach given by Eqs. 9, 10 and Eqs. 19–21 as “variational effective index method” vEIM.

Depending on the actual local refractive index contrast, $\epsilon_{\text{eff}} = N_{\text{eff}}^2$ can well turn out to be negative. This then implies an imaginary effective index N_{eff} , along with evanescent wave propagation, in the respective regions. To circumvent issues related to the signs of N_{eff} for $\epsilon_{\text{eff}} < 0$, we will avoid the term “effective index” in these cases. Note that only ϵ_{eff} appears in the 1-D equations that govern the 1-D problems. Obviously, along with the propagation constant of the reference mode, ϵ_{eff} changes with the vacuum wavelength, or frequency, respectively, (just as the effective index in the slab regions in a standard EIM, Dems and Nakwaski 2006).

Equations 9, 21 represent standard effective index/permittivity values, and modifications thereof. Unlike Yang et al. (2005), Zhou et al. (2007), Liu and Panepucci (2008), here the modifications concern the—formerly undefined—effective properties of the holes only, while the—well defined—effective indices in the non-etched regions remain precisely as in the standard EIM. All effective properties are here derived from first principles, not fitted to numerical reference calculations.

Most of the above expressions [exception: Eqs. 20, 21] are valid for graded index structures as well (van de Velde et al. 1988). Solution of the resulting 1-D problems (10), (19) with continuously varying effective properties ϵ_{eff} , a , b would require suitable (numerical) 1-D solvers in place of the present transfer matrix procedures, if multilayer approximations are to be avoided.

For obvious physical reasons (perpendicular incidence of plane waves on a planar multilayer configuration), polarization does not play any role at the level of the 1-D equations. The positions, where the effective quantities ϵ_{eff} in Eq.10 and a , b in Eq. 19 appear, can be exchanged. To see this, reformulate Eq. 19 and the continuity requirements for ψ and $b^{-1}\partial_z\psi$, for the derivative of the principal function. This leads to the equation

$$\partial_z \frac{1}{a} \partial_z \phi + k^2 b \phi = 0 \tag{23}$$

for $\phi = b^{-1}\psi$, now accompanied by continuity requirements for ϕ and $a^{-1}\partial_z\phi$. Up to the transformation between ψ and ϕ , solutions of Eqs. (19) and (23) should thus be identical. In particular, they predict the same levels of reflection and transmission. Note that this reasoning also covers Eq. 10.

A last remark shall concern the power balance. For a planar configuration, the flux P of optical power per lateral unit length across a plane at position z is given by the integral $P(z) = \text{Re} \int \{E_x H_y^* - E_y H_x^*\} dx$ of the z -component of the Poynting vector. For TE polarized fields of the form (11), this evaluates to

$$P_{\text{TE}} = \frac{1}{2\omega\mu_0} \int |\chi_r|^2 dx \text{Im}(\psi(\partial_z\psi)^*), \tag{24}$$

while one obtains

$$P_{\text{TM}} = \frac{-1}{2\omega\epsilon_0} \int \frac{1}{\epsilon} |\chi_r|^2 dx \text{Im}((\partial_z\psi)\psi^*), \tag{25}$$

for TM fields as in Eq. 22. By using the respective equations that govern ψ , one can show that both $\partial_z P_{\text{TE}}$ and $\partial_z P_{\text{TM}}$ vanish. Thus the 1-D vEIM schemes of Sects. 2.1 and 2.2 generate strictly power conservative solutions.

3 Examples

Sections 3.1–3.4 summarize results of the former procedure, and of “standard” effective index approach(es), for a series of short, high-contrast 2-D structures. One might question in advance whether a 1-D reduction can be useful at all for the parameter sets as considered; in view of the analogy with perturbation theory of first order in the permittivity contrast the examples certainly represent rather extreme cases. Still, we experienced that EIM-like approximations *are* being applied for similar (3-D) PC configurations. Therefore, shedding some light on these scenarios might be more helpful than a discussion of low contrast gratings with shallow etching.

In all configurations there is (at least) one guided slab mode in the non-etched regions; the corresponding vertical refractive index profile thus allows to compute a reasonable effective index which enters both the “conventional” EIM calculations and the vEIM procedures. The non-etched slab also provides the reference permittivity and vertical mode profile to evaluate Eqs. 9, 18, and 21 for the vEIM approach. All configurations have also in common that the etched regions (holes) do not support any guided modes. The “conventional” EIM approach thus requires to guess an effective index for the hole regions; results for different plausible values are compared in the figures.

Along with the vertical mode profiles and with the exception of the former “guessed” values, all effective indices are wavelength dependent. The dependence appears roughly linear for the present configurations; corresponding intervals are given in the text.

A semianalytic Helmholtz solver (quadrilateral eigenmode propagation, QUEP Hammer 2007, 2009) is applied to generate reference solutions for the present 2-D problems. The QUEP results should be more or less converged on the scale of the figures (checked only roughly). Especially for TM polarization the windowing error (Vassallo 1991; Hammer 2007) associated with the eigenmode expansion causes a slightly irregular behavior of the curves; one should not trust the data more than up to the level of these oscillations.

In contrast to the EIM and vEIM approximations, the rigorous QUEP calculations cover vertically propagating waves accurately. This out-of plane scattering manifests through losses in the guided wave power balance, which cannot be taken into account by the EIM and vEIM approximations. One should thus focus the comparison to those spectral regions without pronounced losses, i.e., the regions with bright background in Figs. 2, 4, 5, and 6.

3.1 Deeply etched waveguide grating

Figure 2 introduces a parameter set that could represent a deeply etched, air-covered Si_3N_4 film on a SiO_2 substrate. Results for the polarized spectral guided wave transmission and reflection are compared for different computational approaches. The background shading indicates the level of losses (vertical out of plane scattering) as predicted by the QUEP reference; darker shading indicates higher losses. The gray patches in the left corners of the plots span the wavelength range where the slab is multimode.

Both EIM and vEIM approximations rely on effective indices for the slab segments between $N_{\text{eff}}^{\text{slab}} = 1.87$ ($\lambda = 0.4 \mu\text{m}$) and 1.67 ($\lambda = 0.9 \mu\text{m}$) for TE polarization, and between $N_{\text{eff}}^{\text{slab}} = 1.89$ ($\lambda = 0.3 \mu\text{m}$) and 1.55 ($\lambda = 0.8 \mu\text{m}$) for TM fields. The vEIM effective properties Eqs. (9), (18), (21), in the etched regions vary from $N_{\text{eff}}^{\text{holes}} = 0.82$ ($\lambda = 0.4 \mu\text{m}$) to 0.71 ($\lambda = 0.9 \mu\text{m}$) for TE, and from $N_{\text{eff}}^{\text{holes}} = 0.81$, $b^{\text{holes}} = 0.25$ ($\lambda = 0.3 \mu\text{m}$) to $N_{\text{eff}}^{\text{holes}} = 0.64$, $b^{\text{holes}} = 0.34$ ($\lambda = 0.8 \mu\text{m}$) for TM polarization.

We look first at the TE results, and there at the wavelength range beyond $0.48 \mu\text{m}$ with moderate losses. Three choices for $N_{\text{eff}}^{\text{holes}}$ have been considered, two of which are physically

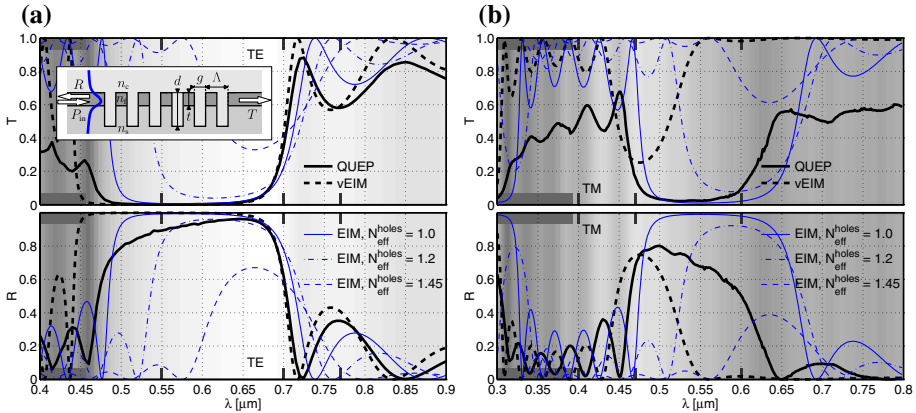


Fig. 2 A deeply etched, vertically nonsymmetric waveguide Bragg grating. Parameters: $n_c = 1.0, n_f = 2.0, n_s = 1.45, t = 0.2 \mu\text{m}, \Lambda = 0.21 \mu\text{m}, g = 0.11 \mu\text{m}, d = 0.6 \mu\text{m}$. Relative guided wave (fundamental mode) transmission T and reflection R versus vacuum wavelength λ , for excitation by TE (a) and TM polarized waves (b). Bold lines QUEP (continuous, reference), vEIM (dashed). Thin curves “conventional” EIM, $N_{\text{eff}}^{\text{holes}} = 1.0$ (continuous), $N_{\text{eff}}^{\text{holes}} = 1.2$ (dash-dotted), $N_{\text{eff}}^{\text{holes}} = 1.45$ (dashed)

motivated, i.e., the refractive indices 1.0 and 1.45 for the air and the substrate that are present in the hole region, while the intermediate value of 1.2 has been included to show the trend. Among these, only the value for air leads to EIM predictions that resemble the QUEP reference reasonably. Probably due to the depth of the holes the substrate value is not adequate here. Especially for the long wavelengths, the vEIM curves come still closer to the reference data.

What concerns TM polarization, the pronounced out of plane losses, indicated by the dark background, render all 1-D approximations almost useless. In principle one observes the same trends as for TE polarized fields, where it is difficult to decide whether to prefer the vEIM data over the EIM results with $N_{\text{eff}}^{\text{holes}} = 1.0$ (both reflection and transmission should be considered). The vEIM procedures at least allow to assemble consistent field approximations via Eqs. 11, 22. Some exemplary profiles are illustrated in Fig. 3, alongside the QUEP results. Also here the high TM losses become evident: In each case, one should compare the levels of outgoing waves surrounding the grating regions with the homogeneous, constant background of the power conservative vEIM simulations.

3.2 High contrast PC membrane

Figure 4 addresses the 2-D equivalent of a thin Si membrane with periodic air holes. Here we restrict to TE polarization, since the identification of a similar, high contrast parameter set that leads to a moderately lossy grating with fully etched holes and single mode access waveguides turns out to be difficult for TM waves.

The effective properties of the non-etched slab for the EIM and vEIM simulations evaluate to $N_{\text{eff}}^{\text{slab}} \in [2.33_{\lambda = 2.2 \mu\text{m}}, 3.09_{\lambda = 0.8 \mu\text{m}}]$. This is an example where the vEIM recipe (9) leads to negative effective permittivity in the etched regions $\epsilon_{\text{eff}}^{\text{holes}} \in [-1.30_{\lambda = 2.2 \mu\text{m}}, -0.41_{\lambda = 0.8 \mu\text{m}}]$. The vEIM model thus predicts a purely evanescent field behavior across the holes.

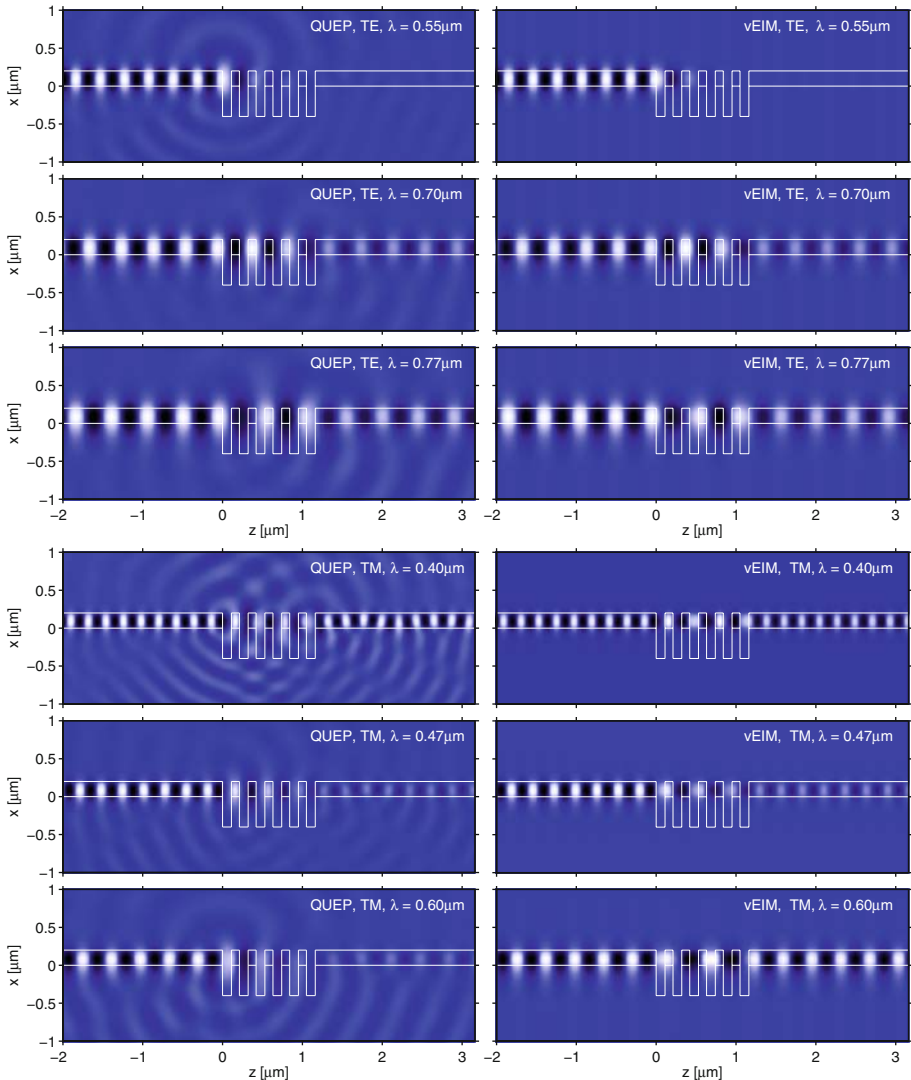


Fig. 3 Field profiles associated with the grating of Fig. 2; time snapshots of the principal electric field component E_y for TE, and magnetic component H_y for TM polarization; QUEP reference calculation and vEIM approximation, for the wavelengths indicated by the *bold tick marks* in Fig. 2

Only the choice of $N_{\text{eff}}^{\text{holes}} = 1.0$ seems plausible for the standard EIM in this case. If we focus to the spectral region $\lambda > 1.3 \mu\text{m}$ with lower losses, the vEIM data comes again moderately closer to reality than the standard EIM.

3.3 Defect cavity

Figure 5 looks at a resonance in an air-clad Si/SiO₂ grating with a central defect. Also here we restrict the simulations to TE polarization.

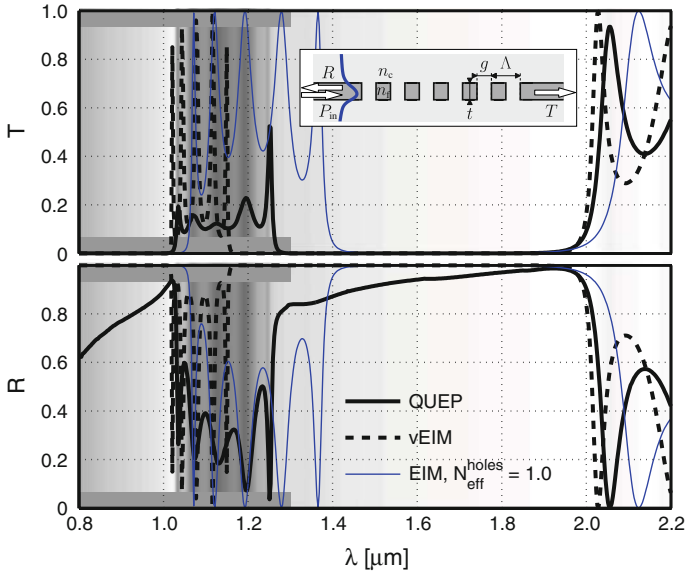


Fig. 4 A high contrast vertically symmetric waveguide Bragg grating. Parameters: $n_c = 1.0$, $n_f = 3.4$, $t = 0.2 \mu\text{m}$, $\Lambda = 0.45 \mu\text{m}$, $g = 0.225 \mu\text{m}$. Modal transmission T and reflection R versus the vacuum wavelength λ , for TE polarized waves. *Bold lines* QUEP (*continuous*, reference), vEIM (*dashed*). *Thin curves* “conventional” EIM, $N_{\text{eff}}^{\text{holes}} = 1.0$

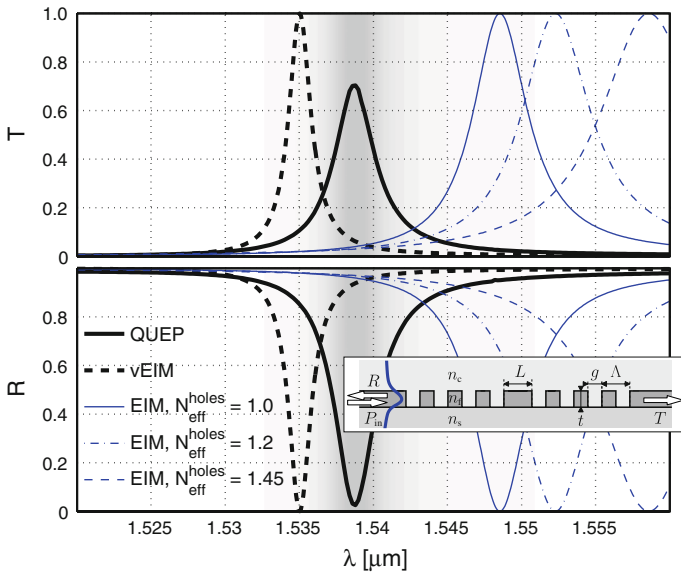


Fig. 5 Vertically nonsymmetric waveguide grating with central defect. Parameters: $n_c = 1.0$, $n_f = 3.4$, $n_s = 1.45$, $t = 0.220 \mu\text{m}$, $\Lambda = 0.310 \mu\text{m}$, $g = 0.135 \mu\text{m}$, $L = 1.515 \mu\text{m}$. Spectral transmission T and reflection R around a defect resonance, for TE polarized excitation. *Bold lines* QUEP (*continuous*, reference), vEIM (*dashed*). *Thin curves* “conventional” EIM, $N_{\text{eff}}^{\text{holes}} = 1.0$ (*continuous*), $N_{\text{eff}}^{\text{holes}} = 1.2$ (*dash-dotted*), $N_{\text{eff}}^{\text{holes}} = 1.45$ (*dashed*)

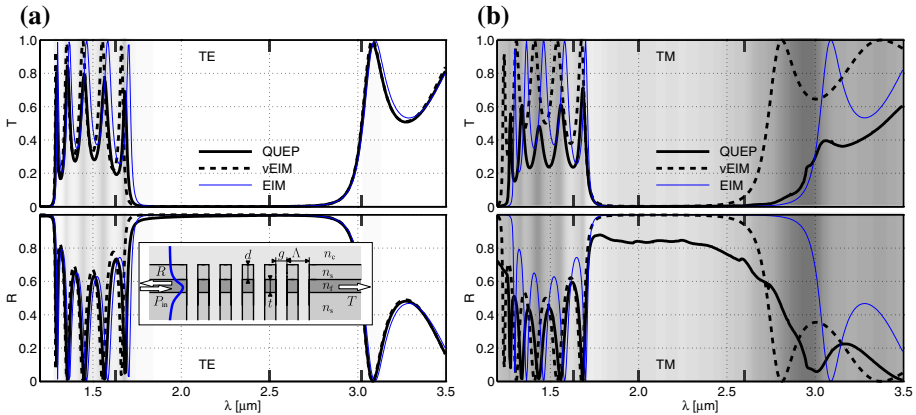


Fig. 6 A Bragg grating with air-filled holes in a heterostructure slab configuration. Parameters: $n_s = 3.1693$, $n_f = 3.3640$, $n_c = 1.0$, $t = 0.5 \mu\text{m}$, $\Lambda = 0.491 \mu\text{m}$, $g = \Lambda/2$, $d = 1.0 \mu\text{m}$. The plots show the relative spectral guided wave transmission T and reflection R , for excitation by TE (a) and TM polarized waves (b). Bold lines QUEP (continuous, reference), vEIM (dashed). Thin curve “conventional” EIM with $N_{\text{eff}}^{\text{holes}} = 1.0$.

There is only a very moderate variation of effective parameters in the narrow wavelength region that is of interest here: $N_{\text{eff}}^{\text{slab}} \in [2.75_{\lambda=1.56 \mu\text{m}}, 2.77_{\lambda=1.52 \mu\text{m}}]$ (vEIM and EIM). Negative values are obtained for the vEIM effective permittivity in the hole regions: $\epsilon_{\text{eff}}^{\text{holes}} \in [-0.96_{\lambda=1.56 \mu\text{m}}, -0.94_{\lambda=1.52 \mu\text{m}}]$.

With the refractive indices 1.0 of the cover and 1.45 of the substrate there are again two reasonable choices for the effective index of the etched regions. Also values in between might be plausible. According to Fig. 5, all of these lead to resonance positions that are further off the QUEP reference than the vEIM prediction.

In line with the observations in Sects. 3.1 and 3.2, with decreasing $\epsilon_{\text{eff}}^{\text{holes}}$ one observes a systematic shift of the spectral features to shorter wavelengths, where the standard EIM values do not proceed far enough, while the vEIM exaggerates slightly. It would thus be tempting to use the resonance position as a measure to for a fit of the effective parameters. This should then concern $\epsilon_{\text{eff}}^{\text{holes}}$, rather *not* the effective index assigned to the slab regions (as in Yang et al. (2005), Zhou et al. (2007), Liu and Panepucci (2008)) which represents exactly the unperturbed guided wave propagation through the non-corrugated regions of the device.

3.4 Heterostructure PC slab

For the last example in Fig. 6, we adapted a parameter set from refs. Kok et al. (2007), Kok (2008), which represents an InP/InGaAsP/InP heterostructure with air cover and deep, air-filled holes. The vertical refractive index contrast around the guiding layer in the original slab is quite low in this case, leading to a comparatively wide, regular vertical mode shape.

EIM and vEIM simulations are based on effective indices for the slab regions of $N_{\text{eff}}^{\text{slab}} \in [3.20_{\lambda=3.5 \mu\text{m}}, 3.29_{\lambda=1.2 \mu\text{m}}]$ (TE), and $N_{\text{eff}}^{\text{slab}} \in [3.19_{\lambda=3.5 \mu\text{m}}, 3.29_{\lambda=1.2 \mu\text{m}}]$ (TM). Effective properties of $\epsilon_{\text{eff}}^{\text{holes}} \in [0.737_{\lambda=3.5 \mu\text{m}}, 0.741_{\lambda=1.2 \mu\text{m}}]$ (TE) and $\epsilon_{\text{eff}}^{\text{holes}} \in [0.741_{\lambda=3.5 \mu\text{m}}, 0.732_{\lambda=1.2 \mu\text{m}}]$, $b_{\text{eff}}^{\text{holes}} \in [0.096_{\lambda=3.5 \mu\text{m}}, 0.090_{\lambda=1.2 \mu\text{m}}]$ (TM) enter the vEIM calculations, while the value of $N_{\text{eff}}^{\text{holes}} = 1.0$ is the only plausible choice for the standard EIM. Due to the narrow region allowed for mode indices between the substrate and film values n_s and n_f , all effective properties vary only slowly in this case.

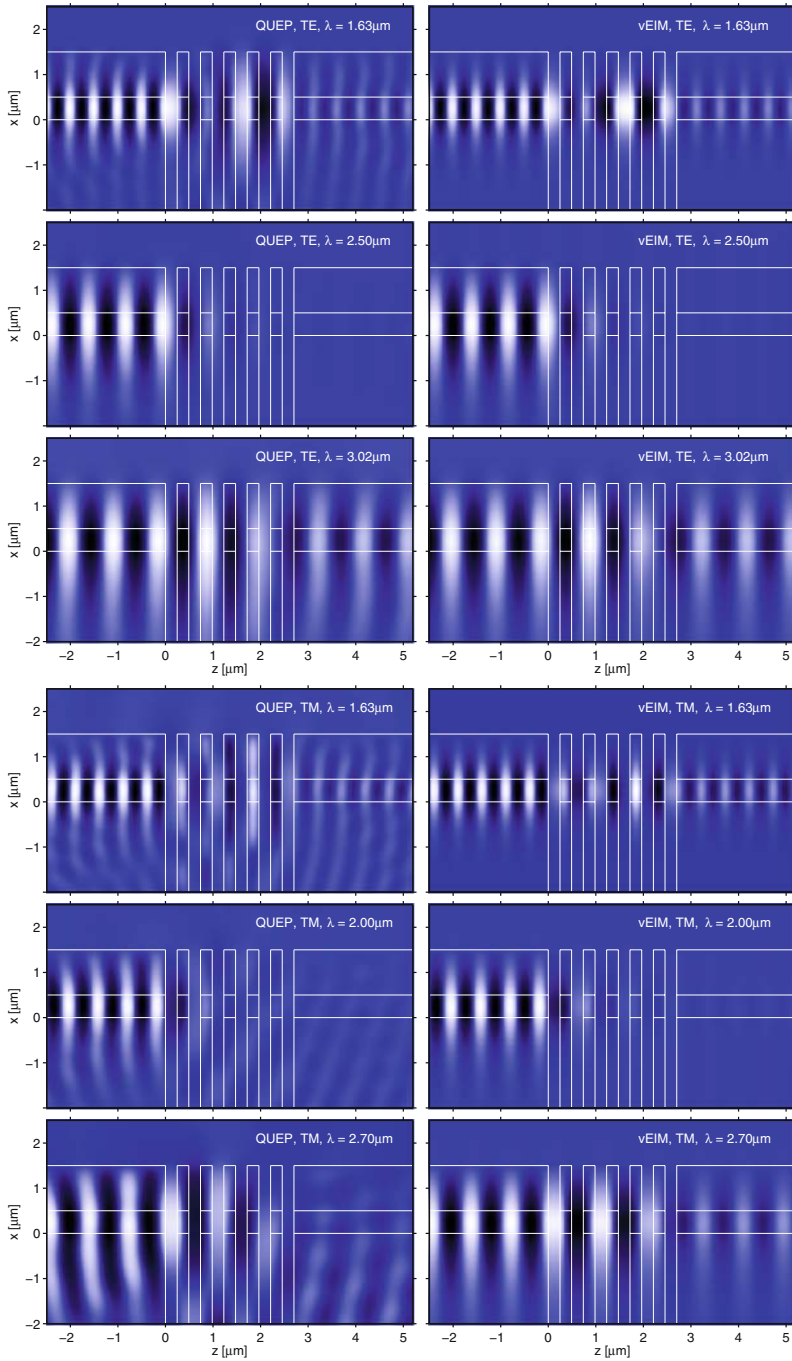


Fig. 7 Field profiles associated with the grating of Fig. 6; time snapshots of the principal electric field component E_y for TE, and magnetic component H_y for TM polarization; QUEP reference calculation and vEIM approximation, for the wavelengths indicated by the bold tick marks in Fig. 6

For TE polarization this is a low-loss configuration. Both vEIM and EIM lead to an excellent approximation of the transmission properties, at least for wavelengths longer than, say, $1.6\ \mu\text{m}$. In case of the vEIM one also obtains quite reasonable approximations of the optical fields, as shown in Fig. 7. The structure exhibits much higher losses for TM waves, and consequently also the quality of the 1-D approximations degrades. Still, the transmission properties around the band edge on the short wavelength side are reasonably well represented by the vEIM and EIM curves. Despite the losses one still observes some agreement between the QUEP and vEIM fields for these wavelengths.

4 Concluding remarks

Our simulations show clearly that a treatment of a propagation problem involving a high-contrast PC slab or PC membrane in terms of effective indices can, in general, hardly be expected to be more than a mere qualitative or rather crude quantitative approximation. Nevertheless, situations may arise where, for various reasons, there are no options but to restrict simulations of 3-D devices to 2-D. One should then at least invest the small effort to determine the variational correction term, and perform the 2-D calculation for the thus established effective permittivity profile (which may well turn out to be smaller than 1.0 locally, or even negative). Some heuristics can be avoided in that way, one obtains clearly defined approximations to the optical fields, and, at least for the given examples with moderate losses, we could observe that the resulting variational effective index approximation (vEIM) comes closer to reality than any “conventional” EIM with educated guesses of effective indices for regions without local modes. The former examples might then give an idea about what accuracy can be expected.

At least for the high contrast configurations among our numerical examples, we could not confirm the rather promising findings of e.g., [Qiu et al. \(2002\)](#) what concerns the validity of standard effective index approximations for photonic crystal slabs in general. Those comparisons considered mainly heterostructure systems as in Sect. 3.4 with relatively low vertical refractive index contrast between a central guiding layer and the thick lower and upper cladding. The shallower mode profile can well be a better approximation to the actual field in the perforating holes than the strongly confined modes in e.g., the PC membrane of Sect. 3.2, such that the standard EIM is more appropriate there than in the previous examples. This would be in line with the findings of [Benisty et al. \(2000\)](#) which predict lower out-of-plane radiation losses for vertical low-contrast heterostructures than for “comparable” high-contrast PC membranes. Quite excellent approximations, as in Fig. 6a, can be obtained in certain cases; the accuracy is, however, strongly structure- and also polarization dependent.

Acknowledgments This work has been supported by the Dutch Technology foundation (BSIK/NanoNed project TOE.7143). The authors thank Brenny van Groesen, Hugo Hoekstra, and Remco Stoffer for many fruitful discussions.

Open Access This article is distributed under the terms of the Creative Commons Attribution Noncommercial License which permits any noncommercial use, distribution, and reproduction in any medium, provided the original author(s) and source are credited.

References

- Benson, T.M., Bozeat, R.J., Kendall, P.C.: Rigorous effective index method for semiconductor rib waveguides. *IEE Proc. J.* **139**(1), 67–70 (1992)
- Benisty, H., Weisbuch, C., Labilloy, D., Rattier, M., Smith, C.J.M., Krauss, T.F., De La Rue, R.M., Houdré, R., Oesterle, U., Jouanin, C., Cassagne, D.: Optical and confinement properties of two-dimensional photonic crystals. *J. Lightwave Technol.* **17**(11), 2063–2077 (1999)
- Benisty, H., Labilloy, D., Weisbuch, C., Smith, C.J.M., Krauss, T.F., Cassagne, D., Béraud, A., Jouanin, C.: Radiation losses of waveguide-based two-dimensional photonic crystals: positive role of the substrate. *Appl. Phys. Lett.* **76**(5), 532–534 (2000)
- Bienstman, P., Assefa, S., Johnson, S.G., Joannopoulos, J.D., Petrich, G.S., Kolodziejski, L.A.: Taper structures for coupling into photonic crystal slab waveguides. *J. Opt. Soc. Am. B* **20**(9), 1817–1821 (2003)
- Blair, S., Goeckeritz, J.: Effect of vertical mode matching on defect resonances in one-dimensional photonic crystal slabs. *J. Lightwave Technol.* **24**(3), 1456–1461 (2006)
- Chiang, K.S.: Analysis of the effective-index method for the vector modes of rectangular-core dielectric waveguides. *IEEE Trans. Microw. Theory Technol.* **44**(5), 692–700 (1996)
- Chiang, K.S.: Analysis of optical fibers by the effective-index method. *Appl. Opt.* **25**(3), 348–354 (1986)
- Čtyrský, J.: Photonic bandgap structures in planar waveguides. *J. Opt. Soc. Am. A* **18**(2), 435–441 (2001)
- Dems, M., Nakwaski, W.: The modelling of high-contrast photonic crystal slabs using the novel extension of the effective index method. *Opt. Appl.* **36**(1), 51–56 (2006)
- Gao, D., Zhou, Z.: Nonlinear equation method for band structure calculations of photonic crystal slabs. *Appl. Phys. Lett.* **88**:163105 (1–3) (2007)
- Gnan, M., Bellanca, G., Chong, H.M.H., Bassi, P., De la Rue, R.M.: Modelling of photonic wire bragg gratings. *Opt. Quantum Electron.* **38**, 133–148 (2006)
- Hadley, G.R.: Out-of-plane losses of line-defect photonic crystal waveguides. *IEEE Photon. Technol. Lett.* **14**(5), 642–644 (2002)
- Hammer, M.: Hybrid analytical/numerical coupled-mode modeling of guided wave devices. *J. Lightwave Technol.* **25**(9), 2287–2298 (2007)
- Hammer, M.: METRIC—Mode expansion tools for 2D rectangular integrated optical circuits. <http://www.math.utwente.nl/~hammer/Metric/> (2009)
- Hammer, M., Ivanova, O.V.: On effective index approximations of photonic crystal slabs. *IEEE/LEOS Benelux Chapter, Proceedings of the 13th Annual Symposium*, pp. 203–206. Enschede, The Netherlands (2008)
- Ivanova, O.V., Hammer, M., Stoffer, R., van Groesen, E.: A variational mode expansion mode solver. *Opt. Quantum Electron.* **39**(10–11), 849–864 (2007)
- Ivanova, O.V., Stoffer, R., Hammer, M., van Groesen, E.: A vectorial variational mode solver and its application to piecewise constant and diffused waveguides. In: *12th International Conference on Mathematical Methods in Electromagnetic Theory MMET08, Odessa, Ukraine, Proceedings*, pp. 495–497 (2008a)
- Ivanova, O.V., Stoffer, R., Hammer, M.: A dimensionality reduction technique for scattering problems in photonics. *1st International Workshop on Theoretical and Computational Nano-Photonics TaCoNa-Photonics, Conference Proceedings*, p. 47 (2008b)
- Ivanova, O.V., Stoffer, R., Hammer, M.: Variational effective index method for 3D vectorial scattering problems in photonics: TE polarization. In: *Proceedings of the Progress in Electromagnetics Research Symposium PIERS 2009, Moscow*, pp. 1038–1042 (2009a)
- Ivanova, O.V., Stoffer, R., Hammer, M.: A variational mode solver for optical waveguides based on quasi-analytical vectorial slab mode expansion. *Opt. Commun.* (2009b) (submitted)
- Kok, A., Geluk, E.J., Docter, B., van der Tol, J., Nötzel, R., Smit, M.: Transmission of pillar-based photonic crystal waveguides in InP technology. *Appl. Phys. Lett.* **91**:201109 (1–3) (2007)
- Kok, A.A.M.: Pillar photonic crystals in integrated circuits. Ph.D. Thesis, Technical University of Eindhoven, Eindhoven, The Netherlands (2008)
- Krauss, T.F., De La Rue, R., Brand, S.: Two-dimensional photonic-bandgap structures operating at near-infrared wavelengths. *Nature* **383**, 699–702 (1996)
- Liu, T., Panepucci, R.R.: Fast estimation of total quality factor of photonic crystal slab cavities. *University/Government/Industry Micro/Nano Symposium UGIM 2008, 17th Biennial, Proceedings*, pp. 233–235 (2008)
- Lohmeyer, M.: Guided waves in rectangular integrated magneto-optic devices. *Cuvillier Verlag, Göttingen, Dissertation, Universität Osnabrück* (1999)
- Lohmeyer, M., Stoffer, R.: Integrated optical cross strip polarizer concept. *Opt. Quantum Electron.* **33**(4/5), 413–431 (2001)
- Lohmeyer, M., Wilkens, L., Zhuromskyy, O., Dötsch, H., Hertel, P.: Integrated magneto-optic cross strip isolator. *Opt. Commun.* **189**(4–6), 251–259 (2001)
- März, R.: *Integrated Optics—Design and Modeling*. Artech House Boston, London (1994)

- Okamoto, K.: *Fundamentals of Optical Waveguides*. Academic Press, San Diego (2000)
- Prather, D.W., Shi, S., Murakowski, J., Schneider, G.J., Sharkawy, A., Chen, C., Miao, B.: Photonic crystal structures and applications: perspective, overview, and development. *IEEE J. Sel. Top. Quantum Electron.* **12**(6), 1416–1437 (2006)
- Qiu, M.: Effective index method for heterostructure-slab-waveguide-based two-dimensional photonic crystals. *Appl. Phys. Lett.* **81**(7), 1163–1165 (2002)
- Qiu, M., Azizi, K., Karlsson, A., Swillo, M., Jaskorzynska, B.: Numerical studies of mode gaps and coupling efficiency for line-defect waveguides in two dimensional photonic crystals. *Phys. Rev. B*, **64**:155113 (1–5) (2001)
- Qiu, M., Jaskorsynska, B., Swillo, M., Benisty, H.: Time domain 2-D modeling of slab-waveguide-based photonic crystal devices in the presence of radiation losses. *Microw. Opt. Technol. Lett.* **34**(5), 387–393 (2002)
- Qiu, M., Mulot, M., Swillo, M., Anand, S., Jaskorzynska, B., Karlsson, A.: Photonic crystal optical filter based on contra-directional waveguide coupling. *Appl. Phys. Lett.* **83**(25), 5121–5123 (2003)
- Shi, S., Chen, C., Prather, D.W.: Revised plane wave method for dispersive material and its application to band structure calculations of photonic crystal slabs. *Appl. Phys. Lett.* **86**:043104 (1–3) (2005)
- Sopaheluwakan, A.: *Characterization and Simulation of Localized States in Optical Structures*. Ph.D. Thesis, University of Twente, Enschede, The Netherlands (2006)
- Taflove, A., Hagness, S.C.: *Computational Electrodynamics: The Finite Difference Time Domain Method*, 2nd edn. Artech House, Norwood (2000)
- van de Velde, K., Thienpont, H., van Geen, R.: Extending the effective index method for arbitrarily shaped inhomogeneous optical waveguides. *J. Lightwave Technol.* **6**(6), 1153–1159 (1988)
- van Groesen, E.: Variational modelling for integrated optical devices. In: *Proceedings of the 4th IMACS-Symposium on Mathematical Modelling*, pp. 5–7. Vienna, Feb (2003)
- van Groesen, E.W.C., Molenaar, J.: *Continuum Modeling in the Physical Sciences*. SIAM, Philadelphia (2007)
- Vassallo, C.: *Optical Waveguide Concepts*. Elsevier, Amsterdam (1991)
- Witzens, J., Lončar, M., Scherer, A.: Self-collimation in planar photonic crystals. *IEEE J. Sel. Top. Quantum Electron.* **8**(6), 1246–1257 (2002)
- Yang, L., Motohisa, J., Fukui, T.: Suggested procedure for the use of the effective-index method for high-index-contrast photonic crystal slabs. *Opt. Eng.* **44**(7):078002 (1–7) (2005)
- Zhou, W., Qiang, Z., Chen, L.: Photonic crystal defect mode cavity modelling: a phenomenological dimensional reduction approach. *J. Phys. D: Appl. Phys.* **40**, 2615–2623 (2007)